THE JOURNAL OF PHYSICAL CHEMISTRY C

Article

pubs.acs.org/JPCC

# Cooperative Upconversion Luminescence Properties of $Yb^{3+}$ and $Tb^{3+}$ Heavily Codoped Silicate Garnet Obtained by Multiple Chemical Unit Cosubstitution

Wenge Xiao,[†,‡] Dan Wu,[†,‡] Liangliang Zhang,*[,†] Xia Zhang,[†] Zhendong Hao,[†] Guo-Hui Pan,[†] Haifeng Zhao,[†] Ligong Zhang,[†] and Jiahua Zhang*[,†]

[†]State Key Laboratory of Luminescence and Applications, Changchun Institute of Optics, Fine Mechanics and Physics, Chinese Academy of Sciences, Changchun 130033, China

[‡]University of Chinese Academy of Sciences, Beijing 100049, China

**ABSTRACT:** As is well-known, the aliovalent substitution level is usually very limited due to the charge mismatch. Particularly, the single phase can hardly be obtained by solid-state reaction for the famous silicate garnet $Ca_3Sc_2Si_3O_{12}$ (CSS), even when the doping level of trivalent rare earth ion ($RE^{3+}$) for $Ca^{2+}$ in CSS is lower than 2 mol %, which largely restricts CSS to be an ideal host for $RE^{3+}$-activated luminescence materials especially where high doping concentration is required. Herein, by using the strategy of multiple chemical unit cosubstitution, we obtained $RE^{3+}$ heavily doped single-phase CSS via the sol−gel method followed by high-temperature sintering. Multiple chemical unit substitutions of [$REO_8$], [$AlO_6$], and [$AlO_4$], respectively, for [$CaO_8$], [$ScO_6$], and [$SiO_4$] polyhedra can act as charge compensators for each other to promote the doping level of $RE^{3+}$ up to 20 mol %, which is high enough for most of the $RE^{3+}$-doped luminescence materials. Moreover, intense cooperative upconversion (UC) luminescence (UCL) was observed in $Yb^{3+}$ and $Tb^{3+}$ codoped CSS, whose intensity is 37 times higher than that of the reported $Y_3Al_5O_{12}$ with garnet structure as well, making it a potential candidate for optical applications like a tunable UC laser. The results show that the preferred formation of the $Yb^{3+}$−$Yb^{3+}$ pair in CSS can largely enhance the efficiency of the cooperative UC process. Besides, the UCL properties were investigated in detail to understand the UC processes and the underlying energy transfer mechanisms. It is confirmed that the multiple chemical unit cosubstitution is an effective strategy to promote the aliovalent substitution level or design solid solution materials to enhance or tune the luminescence properties where relatively high doping concentration is required.

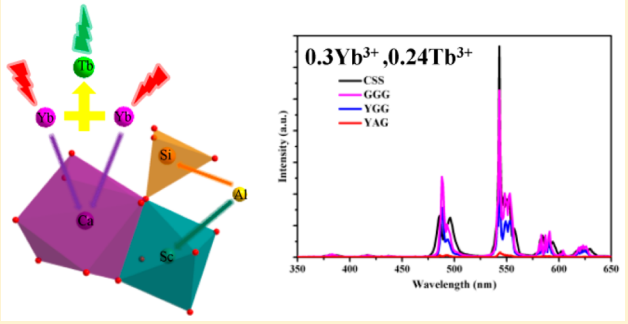


## 1. INTRODUCTION

Recently, upconversion (UC) luminescence (UCL) in which two or more low-energy photons are converted into a higher-energy photon has attracted much attention due to its potential applications in UC laser and biomarkers.[1−3] Strong UCL has been achieved in $Er^{3+}$, $Ho^{3+}$, and $Tm^{3+}$ activated materials based on the so-called stepwise UC, covering various emission bands from near-infrared (NIR) to visible to ultraviolet (UV).[1−7] In general, $Yb^{3+}$ is used as the sensitizers in UC systems because of the high absorption cross-section and simple energy level diagram. Relatively high doping concentration of $Yb^{3+}$ is usually required to maintain fast energy migration among the donors, allowing efficient energy transfer from the donor to the acceptor. It is well-known that $Tb^{3+}$-doped materials, especially when codoped with $Ce^{3+}$ as the sensitizer, can emit intense green light peaking around 544 nm under UV light excitation as a result of its predominant $^5D_4$−$^7F_5$ transition, which have been widely used as green phosphors for fluorescent lamps as well as white light-emitting diodes (LEDs).[8−11] Moreover, the long-lived upper level $^5D_4$ has low multiphonon loss due to a large energy gap away from the lower $^7F_0$ level. Since the $^7F_5$ level is about 2000 $cm^{-1}$ higher than the ground $^7F_6$ level, the $^5D_4 \rightarrow {}^7F_5$ transition of $Tb^{3+}$ can act as a four-level laser system that requires lower power pump sources. Hence, $Tb^{3+}$-doped materials have also been considered as potential candidates for tunable lasers. When pumping the $^5D_4$ level at 488 nm, the green laser operation of $Tb^{3+}$ has been reported by many researchers, and the yellow laser operation around 585 nm due to the $^5D_4 \rightarrow {}^7F_4$ transition was also obtained for the first time by Metz et al.[12−14] However, as the 488 nm is used as the pumping wavelength, it has been found that excited-state absorption (ESA) at 488 nm from the $^5D_4$ level to the 5*d* band of $Tb^{3+}$ reduces the laser efficiency considerably and even impedes laser operation completely.[14−16]

**Received:** November 18, 2016
**Revised:** January 7, 2017
**Published:** January 13, 2017





DOI: 10.1021/acs.jpcc.6b11633
J. Phys. Chem. C 2017, 121, 2998−3006

To address the above issue, one of the possible approaches is to introduce $Yb^{3+}$ into $Tb^{3+}$-doped materials, whose absorption band is in the NIR region, to suppress the undesired ESA process substantially.[17−19] As schematically illustrated in Figure 1, in the $Yb^{3+}$−$Tb^{3+}$ codoped system, under the excitation of

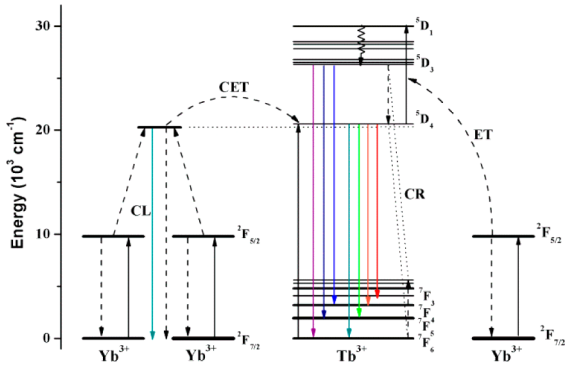


**Figure 1.** Schematic illustration of energy transfer processes and upconversion emissions for the $Tb^{3+}$ and $Yb^{3+}$ codoped system. CL denotes cooperative luminescence, CET cooperative energy transfer, CR cross-relaxation, and ET energy transfer.

980 nm two excited $Yb^{3+}$ simultaneously transfer their energy to a $Tb^{3+}$, and thus $Tb^{3+}$ is excited to the $^5D_4$ level leading to visible luminescence, which has been clearly assigned to a phonon-assisted cooperative energy transfer (CET).[20,21] In addition, two excited $Yb^{3+}$ can simultaneously undergo deexcitation and emit one photon centered at 500 nm whose energy is nearly twice the energy of the normal transition $^2F_{5/2} \rightarrow {}^2F_{7/2}$. This phenomenon is known as cooperative luminescence (CL).[22,23] The two cooperative processes both result from the $Yb^{3+}$−$Yb^{3+}$ pairs coupled by multipolar or super exchange mechanisms and thus are strongly dependent on interionic distances, leading to much higher efficiency for the neighboring $Yb^{3+}$ ions.[24−27] It means that cooperative processes are highly favored in heavily $Yb^{3+}$-doped materials or $Yb^{3+}$−$Yb^{3+}$ pair forming materials, as reported in the literature.[22−33] For this reason, in addition to its potential applications in three-dimensional (3D) display and intrinsic bistability for optical switching, CL of the $Yb^{3+}$−$Yb^{3+}$ pair has been proposed as a probe of clustering in optical materials.[34−37]

Crystals with garnet structure are a group of important optical materials for many advantages such as high chemical and thermal stability and unique optical properties. Particularly, since the garnet structure belongs to the cubic system, providing the optically isotropic properties, garnet-type materials can be made into highly dense polycrystalline ceramics with good transparency even in the visible spectral region and have been successfully applied in the fields of solid state lasers, scintillators, and white LEDs.[38−40] Moreover, because of the rigidity and flexibility of the garnet structure, a number of derivative materials with garnet structure have been reported as potential phosphors for white LEDs as well as solid-state electrolyte for high energy density batteries.[10,41−44]

Silicate garnet $Ca_3Sc_2Si_3O_{12}$ (CSS) when doped with $Ce^{3+}$ has been reported to be a blue-excitable green phosphor with high quantum efficiency and thermal stability.[44] However, single-phase CSS can hardly be obtained by solid state reaction due to the low chemical reactivity of $Sc_2O_3$.[44−47] What's worse, the solubility of a trivalent rare earth ion ($RE^{3+}$) in CSS is very limited (lower than 2 mol %) because there exists charge mismatch between $Ca^{2+}$ and $RE^{3+}$ and the compound series $Ca_3RE_2Si_3O_{12}$ do not possess a cubic crystal structure but an orthorhombic one except for the case of $Sc^{3+}$.[44,48] These problems largely restrict CSS to be used as an ideal host for $RE^{3+}$-activated luminescence materials, especially where heavy doping is required.

In the present work, we have successfully obtained a series of single-phase limited solid solution phosphors between silicate garnet CSS and aluminate garnet $RE_3Al_3O_{12}$ (REAG) via the sol−gel method followed by high-temperature sintering. As will be shown, multiple chemical unit substitutions of [$REO_8$], [$AlO_6$], and [$AlO_4$], respectively, for [$CaO_8$], [$ScO_6$], and [$SiO_4$] polyhedra can act as charge compensators for each other to largely promote the doping level of $RE^{3+}$ replacing $Ca^{2+}$ up to 20 mol %. Furthermore, in $Yb^{3+}$ and $Tb^{3+}$ heavily codoped CSS, efficiency cooperative UCL is observed, and the UC processes are also discussed in detail based on the emission spectra, the pump power dependence of the emission intensity, and the fluorescence decay curves.

## 2. EXPERIMENTAL SECTION

**2.1. Materials and Synthesis.** Several series of solid solution phosphors between CSS and REAG (RE = Tb, Yb, Lu, and Y) were synthesized via the sol−gel method followed by high-temperature sintering. Typically, the high purity raw materials $CaCO_3$ (G.R.), $Sc_2O_3$ (5 N), and $Yb_2O_3$ (6 N) were dissolved into $HNO_3$ (G.R.) to obtain $Ca(NO_3)_2$, $Sc(NO_3)_3$, and $Yb(NO_3)_3$ nitrate solutions, respectively. For the series of samples $Ca_{3(1-x)}Yb_{3x}Sc_{2(1-x)}Al_{2x}Si_{3(1-x)}Al_{3x}O_{12}$ (CSS:3$x$Yb), the stoichiometric amounts of the obtained metal nitrate solutions and $Al(NO_3)_3{\cdot}9H_2O$ (A.R.) were continuously stirred for about 30 min, and in the meantime tetraethoxysilane (TEOS, A.R.) was dissolved in anhydrous ethanol (A.R.). Subsequently, the above-mentioned solutions were mixed for another 30 min. The resulting solution was heated in a dry oven at 65 °C until a transparent gel was obtained after gradual polymerization, which was then further dried at 95 °C to obtain a xerogel. The xerogel was preheated at 700 °C in a muffle furnace for 3 h to remove organic components. After grinding, the precursor was put into an alumina crucible and sintered at 1380 °C in air atmosphere. The synthesized product was reground into fine powders for characterizations, and other series samples singly or doubly doped with $RE^{3+}$ ions were prepared in the same way as described above.

**2.2. Characterization.** Powder X-ray diffraction (XRD) patterns of all samples were collected on a Bruker D8 Focus diffractometer, in the $2\theta$ range from 10° to 80° with Cu K$\alpha$ radiation ($\lambda$ = 1.54056 Å) operating at 40 kV and 30 mA. The scanning rate was 1 s per step with a step size of 0.02°. Structure refinement was carried out by the Rietveld method using the FullProf program.[49] The UC emission spectra were measured using a FLS920 spectrometer (Edinburgh Instruments) pumped with a power controllable 980 nm laser diode. In fluorescence decay curve measurements, an optical parametric oscillator (OPO) was used as an excitation source, and the signal was detected by a Tektronix digital oscilloscope (TDS 3052). All the measurements were conducted at room temperature.

## 3. RESULTS AND DISCUSSION

**3.1. Single-Phase Formation and Structural Characteristics.** Since CSS:Ce may serve as the green phosphor for


DOI: 10.1021/acs.jpcc.6b11633
J. Phys. Chem. C 2017, 121, 2998−3006

white LEDs, great efforts have been made to obtain single-phase CSS:Ce in order to enhance the emission intensity.[44−47] Besides wet-chemical methods, codoping $Al^{3+}$ into CSS:Ce can also inhibit the formation of the impurity phases $Sc_2O_3$ and silicates of calcium to produce single-phase CSS:Ce when the doping $Ce^{3+}$ concentration is relatively low (below 2 mol %). As discussed by Wu et al., as the substitution level of $Sc^{3+}$ by $Al^{3+}$ exceeds 10 mol %, secondary phase $Ca_3Al_2Si_3O_{12}$ (CAS) will arise, belonging to garnet structure as well.[47] Nevertheless, such a garnet-type phase is a high-pressure phase and can be prepared only under high pressure (above 1 GPa);[50] accordingly, in this case the solid solubility of $Al^{3+}$ is very limited in CSS at atmospheric pressure. It is reasonable to expect that some of $Al^{3+}$ may also enter the $Si^{4+}$ site due to their similarities in ionic radius and electronegativity. As is well-known, the general stoichiometric formula of the garnet-type crystal is $\{X\}_3[Y]_2(Z)_3O_{12}$, where {X}, [Y], and (Z) denote dodecahedral (24c), octahedral (16a), and tetrahedral (24d) sites, respectively.[51−53] For CSS, $Ca^{2+}$ ions occupy dodecahedral sites, $Sc^{3+}$ octahedral sites, and $Si^{4+}$ tetrahedral sites, as illustrated in Figure 2a.[44,52] Meanwhile, for REAG, $RE^{3+}$ ions

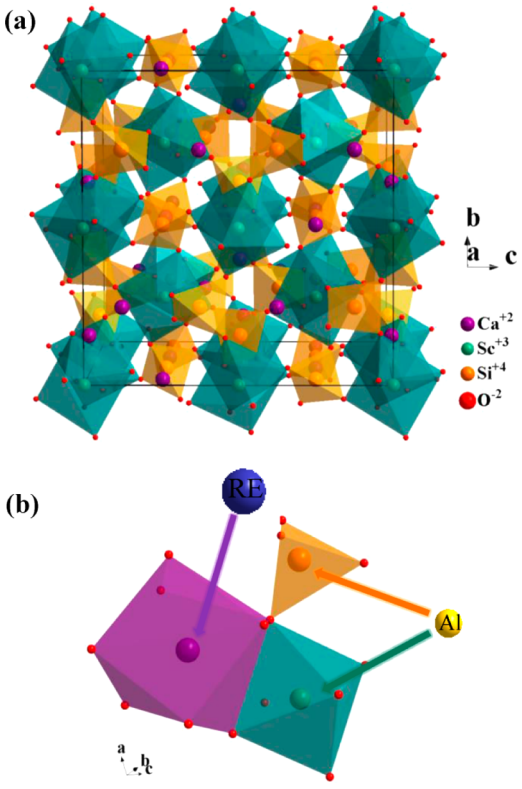


**Figure 2.** (a) Crystal structure of CSS. (b) Proposed multiple chemical unit cosubstitution strategy of $[AlO_6]$, $[AlO_4]$, and $[REO_8]$ stoichiometrically for $[ScO_6]$, $[SiO_4]$, and $[CaO_8]$, respectively.

occupy dodecahedral sites; two of the $Al^{3+}$ ions occupy octahedral sites; and the remaining three occupy tetrahedral sites.[51] Considering the above occupation of the cations, we believe that the amount of $Al^{3+}$ entering the $Si^{4+}$ site could be largely promoted if the local electroneutrality is achieved by some forms of charge balance such as the substitution of $RE^{3+}$ for $Ca^{2+}$. Therefore, we try to use the strategy of chemical unit cosubstitution, which has been widely employed to design color-tunable solid solution phosphors, to obtain $RE^{3+}$ heavily doped single-phase CSS.[41,42,53−56] In our strategy, we designed a multiple chemical unit cosubstitution (see Figure 2b) where three units $[AlO_6]$, $[AlO_4]$, and $[REO_8]$ stoichiometrically replace $[ScO_6]$, $[SiO_4]$, and $[CaO_8]$, respectively, which means that a double substitution of $[AlO_6]$ and $[AlO_4]$, respectively, for $[ScO_6]$ and $[SiO_4]$ acts as charge compensation for $[REO_8]$ replacing $[CaO_8]$ to increase the doping level of $RE^{3+}$ at the $Ca^{2+}$ site in CSS.

The representative XRD patterns of the as-synthesized samples CSS:3$x$RE (RE = Tb, Yb, Lu, and Y) with $x$ = 0.2 are shown in Figure 3a. It can be found that these samples are isostructural with CSS and can be well indexed to the space group $Ia\bar{3}d$ of the cubic system, and no diffraction peaks of impurities are detected, indicating the formation of single-phase solid solution. Nevertheless, it is noteworthy that the solubility of $RE^{3+}$ is largely reduced to lower than 5 mol % ($x$ = 0.05) when its radius is larger than that of $Gd^{3+}$, and for the smaller one ($Gd^{3+}$ to $Y^{3+}$), impurity phases likewise come into being when $x$ exceeds 0.2; these data are not shown here. Generally, the stability of the garnet structure is highly dependent upon the sizes of the substituent cations. For instance, the aluminate garnet REAG is thermodynamically unstable for the case that $RE^{3+}$ is larger than $Gd^{3+}$ ($La^{3+}$ to $Eu^{3+}$), and as mentioned above, the silicate compound $Ca_3RE_2Si_3O_{12}$ does not belong to garnet structure except for the smallest one $Sc^{3+}$; meanwhile silicate garnet CAS can be obtained only under high pressure.[48,50,51] Therefore, in our opinions, qualitatively, further expansion or contraction, respectively, by the introduction of larger $RE^{3+}$ into the {X} site or more $Al^{3+}$ into the [Y] site will both destabilize the formation of the garnet structure.[48,50−52] Fortunately, the achieved doping level is already up to 20 mol % ($x$ = 0.2), which is high enough for most of the $RE^{3+}$-doped luminescence materials.

In order to further investigate the single-phase garnet structure of the as-synthesized samples, the Rietveld structural refinements for the compositions of CSS:3$x$Yb ($x$ = 0, 0.05, 0.1, 0.2), as a representative one, were performed by using the previously reported crystallographic data of CSS as a starting model.[44] Typically, in CSS crystal, the $[ScO_6]$ octahedron and $[SiO_4]$ tetrahedron connect with each other by sharing $O^{2-}$ corners to form the three-dimensional network, and dodecahedral coordinated $Ca^{2+}$ occupies the interstitial position. More specifically, each $[ScO_6]$ is connected to six $[SiO_4]$, while each $[SiO_4]$ is connected to four $[ScO_6]$; from the point of $Ca^{2+}$, every $[CaO_8]$ is surrounded by four $[CaO_8]$, four $[ScO_6]$, and six $[SiO_4]$; accordingly, every $O^{2-}$ coordinated to $Ca^{2+}$ is shared by two $Ca^{2+}$, one $Sc^{3+}$, and one $Si^{4+}$. In our refinements, $Yb^{3+}$ was assumed to occupy the $Ca^{2+}$ site and $Al^{3+}$ to partly occupy the $Sc^{3+}$ site and partly $Si^{4+}$ sites, whose occupancies were fixed according to the nominal chemical formulas. The observed, calculated, and difference patterns of the XRD refinement of CSS:3$x$Yb ($x$ = 0.05, 0.1, 0.2) are shown in Figure 3. The crystallographic data and refinement parameters are listed in Table 1. The final weighted $R$ factors ($R_{wp}$) of all the samples are acceptable, thus confirming the phase purity of these samples. It is unexpected that the shift of the diffraction peaks of the samples CSS:3$x$Yb is negligible with increasing $x$, and correspondingly, the refined unit cell parameters changes little within errors. This can be explained that the substitution of $[AlO_4]$ for $[SiO_4]$ counteracts with the substitutions $[YbO_8]$ for $[CaO_8]$ and $[AlO_6]$ for $[ScO_6]$ in changing the lattice parameters since the $Yb^{3+}$ ion ($r$ = 0.99 Å when coordination number (CN) = 8) is smaller than the $Ca^{2+}$ ion ($r$ = 1.12 Å


DOI: 10.1021/acs.jpcc.6b11633
J. Phys. Chem. C 2017, 121, 2998−3006

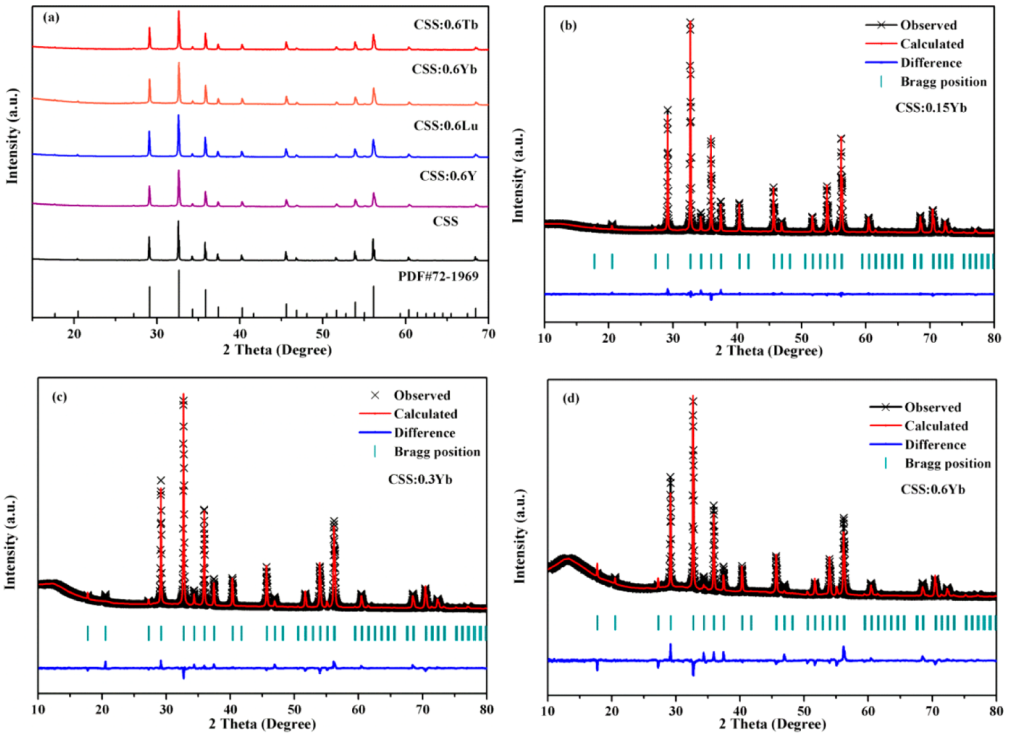


**Figure 3.** (a) XRD patterns of CSS and CSS:0.6RE (RE = Tb, Yb, Lu, and Y). The standard data for CSS (PDF#72-1969) are shown as a reference. (b) Rietveld refinements of XRD data for CSS:0.15Yb. (c) Rietveld refinements of XRD data for CSS:0.3Yb. (d) Rietveld refinements of XRD data for CSS:0.6Yb.

**Table 1. Rietveld Refinement and Crystallographic and Structure Parameters of the Representative Samples CSS:3*x*Yb (*x* = 0, 0.05, 0.1, and 0.2)**

| compound | $x = 0$ | $x = 0.05$ | $x = 0.1$ | $x = 0.2$ |
|---|---|---|---|---|
| space group | $Ia\bar{3}d$ | $Ia\bar{3}d$ | $Ia\bar{3}d$ | $Ia\bar{3}d$ |
| $a = b = c$ (Å) | 12.2499(5) | 12.2437(6) | 12.2438(2) | 12.2432(1) |
| $\alpha = \beta = \gamma$ (deg) | 90 | 90 | 90 | 90 |
| $V$ (Å$^3$) | 1838.24(2) | 1835.46(0) | 1835.48(4) | 1835.21(1) |
| $Z$ | 8 | 8 | 8 | 8 |
| $R_p$ (%) | 3.82 | 3.19 | 3.42 | 4.41 |
| $R_{wp}$ (%) | 5.32 | 4.43 | 5.18 | 7.14 |
| $R_{exp}$ (%) | 2.36 | 2.44 | 1.70 | 2.39 |
| $\chi^2$ | 5.09 | 3.31 | 9.31 | 8.9 |

when CN = 8). $Al^{3+}$ ($r$ = 0.54 Å when CN = 6) is smaller than $Sc^{3+}$ ($r$ = 0.75 Å when CN = 6), while the $Al^{3+}$ ($r$ = 0.39 Å when CN = 4) is larger than $Si^{4+}$ ($r$ = 0.26 Å when CN = 4).[57]

**3.2. UCL Properties of $Tb^{3+}$ and $Yb^{3+}$-Codoped CSS.** The emission spectra of the three representative samples $Ca_{3(0.9-y)}Yb_{0.3}Tb_{3y}Sc_{2(0.9-y)}Al_{2(0.1+y)}Si_{3(0.9-y)}Al_{3(0.1+y)}O_{12}$ (CSS:0.3Yb,3*y*Tb) ($y$ = 0.001, 0.0033, 0.01) under the excitation of 980 nm diode laser with the power of 330 mW are shown in Figure 4a. In order to present the change of the relative intensity of different emission peaks more clearly, we have normalized the spectra by the intensity of 543 nm. It is found that the spectra consist of seven emission peaks centered at 383, 418, 437, 486, 543, 584, and 623 nm, which are attributed to the radiative transitions of $^5D_3 \rightarrow {}^7F_J$ ($J$ = 6, 5, and 4) and $^5D_4 \rightarrow {}^7F_J$ ($J$ = 6, 5, 4, and 3) of the $Tb^{3+}$ ion, respectively, as indicated in Figure 4a. As far as we know, only a handful of papers have evidently observed the emissions from the $^5D_3$ level.[28−33] For the samples with low $Tb^{3+}$ concentration ($y$ = 0.001 and 0.0033), obviously, there is an extra broad emission band around 505 nm, whose relative intensity gradually decreases and almost disappears when $y$ = 0.01. We ascribed this to the CL of the $Yb^{3+}$−$Yb^{3+}$ pair, as will be further discussed below. The concentration dependence of the UCL intensity of the series of samples CSS:0.3Yb,3*y*Tb with $y$ increasing from $y$ = 0.001 to $y$ = 0.1 is depicted in Figure 4b (red line). As the $Tb^{3+}$ concentration increases, the UCL intensity of CSS:0.3Yb,3*y*Tb increases first and reaches its maxima when $y$ = 0.08 and then decreases due to the concentration quenching effect. Furthermore, the changing trend of the two representative emission peaks centered at 383 (blue line) and 543 nm (green line) originating, respectively, from the levels $^5D_3$ and $^5D_4$ are also presented in Figure 4b as a function of $Tb^{3+}$ concentration. One can find that the $^5D_3$ level and $^5D_4$ level have different quenching behaviors as to the $Tb^{3+}$ concentration. For the $^5D_3$ level, the concentration quenching occurs at $y$ = 0.02, while for the $^5D_4$ level it occurs at a much higher doping level ($y$ = 0.08). This can be explained that, in addition to the energy loss at a quenching center through energy migration among $Tb^{3+}$ ions, the excited $^5D_3$ level suffers from strong self-quenching due to cross-relaxation between the


DOI: 10.1021/acs.jpcc.6b11633
J. Phys. Chem. C 2017, 121, 2998−3006

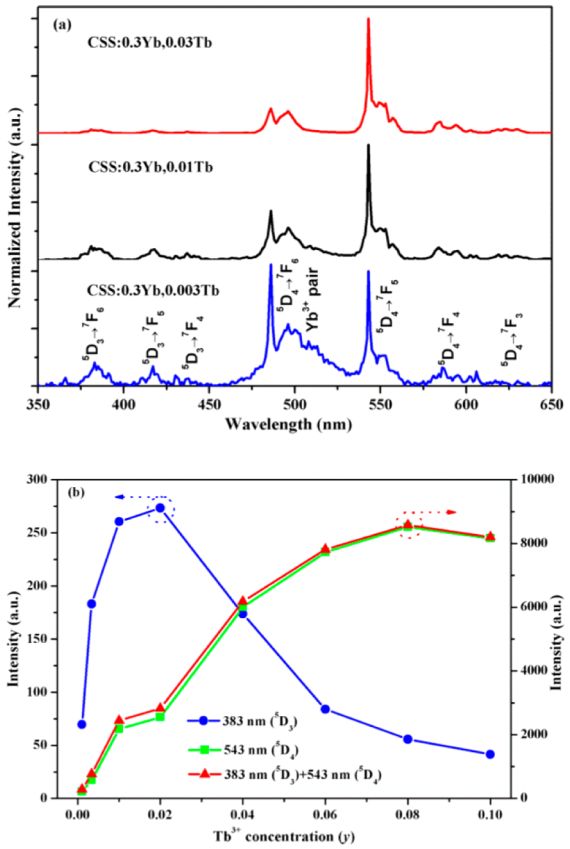


**Figure 4.** (a) UC emission spectra of the three representative samples (CSS:0.3Yb,3*y*Tb) ($y$ = 0.001, 0.0033, 0.01) under the excitation of 980 nm diode laser with the power of 330 mW. (b) Dependence of the UCL intensity of CSS:0.3Yb,3*y*Tb on $Tb^{3+}$ concentration ($y$).

$^5D_3$ level and $^5D_4$ level ($Tb^{3+}(^5D_3)$ + $Tb^{3+}$ ($^7F_6$) → $Tb^{3+}$ ($^5D_4$) + $Tb^{3+}$ ($^7F_J$)) at a higher $Tb^{3+}$ concentration, in favor of the population of $^5D_4$.[28−30]

As for the observed broad emission band around 505 nm in the samples CSS:0.3Yb,3*y*Tb ($y$ = 0.001 and 0.0033) (see Figure 4a), we readily assigned it to the CL of the $Yb^{3+}$−$Yb^{3+}$ pair since the corresponding value in energy is nearly twice that of the normal transition $^2F_{5/2}$ → $^2F_{7/2}$ of single $Yb^{3+}$, and no other $RE^{3+}$ ion has such a broad band in this range.[3,22−24] Note that in the 10 mol % $Yb^{3+}$-doped YAG whose structure is the same as CSS the observation of CL is rather difficult by the influence of unwanted impurities despite using high purity (5 N) starting materials.[27,35] In addition, the minimum Yb−Yb distance in CSS is slightly larger than in YAG (3.75 Å in CSS and 3.67 Å in YAG).[35,44] Considering that the efficiency of CL is strongly dependent on interionic distances, we infer that the formation of the $Yb^{3+}$−$Yb^{3+}$ pair is relatively favored in CSS crystal compared with in YAG. From the perspective of crystal structure, two possible reasons are given as follows. It is considered that antisite defects are more likely to happen when two lattice sites are similar in size. For instance, the occurrence of the antisite defect that $Y^{3+}$ occupies the octahedral site which is supposed to be occupied by $Ga^{3+}$ or $Al^{3+}$ has much higher possibility in $Y_3Ga_5O_{12}$ (YGG) than in YAG.[51,52,58] Accordingly, in CSS, some $Yb^{3+}$ ions are likely to enter [$ScO_6$] octahedrons, resulting in more closely paired $Yb^{3+}$ ions with Yb−Yb distance of 3.42 Å. Besides, although the introduction of $Al^{3+}$ at the $Si^{4+}$ site is able to compensate the excess positive charge by the substitution $Yb^{3+}$ for $Ca^{2+}$ in CSS, it is still possible that there exists a charge compensation mechanism that two $Yb^{3+}$ ions and one $Ca^{2+}$ vacancy replace three $Ca^{2+}$ ions neighboring each other to maintain local electrical neutrality, which has been reported in $Ce^{3+}$-doped CSS as well as in other $RE^{3+}$-doped crystals like $Yb^{3+}$-doped $CaNb_2O_6$ and $Yb^{3+}$-doped $CsCdBr_3$.[20,24,34,59−61] This makes a minority of $Yb^{3+}$ ions to tend to cluster into pairs with shorter Yb−Yb distances than that of the normal random distribution. It follows that the preferred formation of the $Yb^{3+}$−$Yb^{3+}$ pair in CSS is mainly responsible for the intense CL. Such a fact also may benefit the CET from $Yb^{3+}$ to $Tb^{3+}$. As shown in Figure 5,

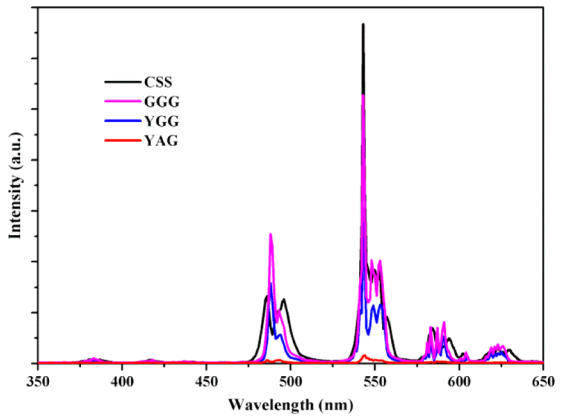


**Figure 5.** Comparison of the UCL intensity of CSS:0.3Yb,0.24Tb with YAG, YGG, and GGG with the same doping concentrations, under the same excitation condition of 980 nm laser.

we further compared the UCL intensity of CSS:0.3Yb,0.24Tb, with the three reported garnets YAG, YGG, and $Gd_3Ga_3O_{12}$ (GGG) with the same doping concentrations.[31,33] One can find that the UCL is the strongest in CSS:0.3Yb,0.24Tb and decreases in sequence from GGG to YAG, especially that it is 37 times stronger in CSS than in YAG as expected. Keep in mind that these materials have the same structure and similar cutoff phonon energies (around 800 $cm^{-1}$), and thus the difference of the multiphonon nonradiatitive transition probabilities of the upper $^2F_{5/2}$ level of $Yb^{3+}$ is neglectable in these materials since there exists an energy gap of 10 000 $cm^{-1}$ between the upper $^2F_{5/2}$ level and the ground $^2F_{7/2}$ level and at least 12 phonons are involved in the multiphonon relaxation.[62,63]

### 3.3. UC Mechanism of $Tb^{3+}$ and $Yb^{3+}$-Codoped CSS.

To identify the energy transfer mechanism involved in the population of the $^5D_4$ and $^5D_3$ states of the $Tb^{3+}$ ions and confirm the CL around 505 nm, the dependence of the fluorescence intensity on the pump power was analyzed and is plotted in double-logarithmic coordinates (see Figure 6). Briefly, the UCL intensity, $I_{em}$, is proportional to the power $n$ of the NIR pump power, and $n$ is the number of excited $Yb^{3+}$ ions involved in the process which is obtained from the relation, $I_{em} \propto P_{NIR}^{n}$.[24,28,29,64] Via linear fitting, the obtained $n$ values are 0.98, 1.80, 1.86, and 2.48 for the emissions at 1040, 543, 505, and 383 nm, respectively, meaning that the fluorescence intensities of the emissions at 505 and 543 nm both show quadratic dependence upon the pump power, and that of the emission at 383 nm is cubically dependent upon the pump power. Accordingly, the populations of the $^5D_4$ and $^5D_3$ levels are two-photon and three-photon UC processes, respectively. As illustrated in Figure 1, the UC mechanisms


DOI: 10.1021/acs.jpcc.6b11633
J. Phys. Chem. C 2017, 121, 2998−3006

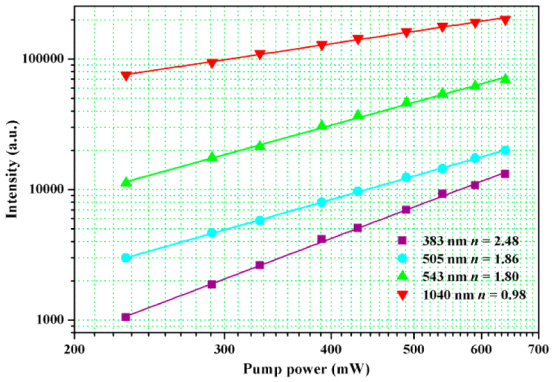


**Figure 6.** Log–log plots of the UCL intensity of CSS:0.3Yb,0.003Tb as a function of the pump power of the 980 nm laser.

can be explained as follows. Upon the excitation of 980 nm, the $Tb^{3+}$ ion is populated to the $^5D_4$ level by phonon-assisted CET from two excited $Yb^{3+}$ ions.[20,21] Subsequently, the excited $Tb^{3+}$ ions relax radiatively to the lower levels $^7F_J$ ($J$ = 6, 5, 4, and 3), resulting in the emission peaks at 486, 543, 584, and 623 nm, respectively. Besides, $Tb^{3+}$ ions in the $^5D_4$ level could be further pumped to the higher $^5D_1$ level by absorbing another photon, i.e., ESA or energy transfer from a third excited $Yb^{3+}$ ion, and then relax nonradiatively to the $^5D_3$ level. Finally, a part of those excited $Tb^{3+}$ ions generates emission peaks at 383, 418, and 437 nm by transitions of $^5D_3 \rightarrow {}^7F_J$ ($J$ = 6, 5, and 4), respectively. The rest will go back to the $^5D_4$ level partly via multiphonon relaxation and partly, especially at high $Tb^{3+}$ concentrations, via cross-relaxation energy transfer, leading to the enhancement of the green emission relative to the UV emission as described above. For the emission around 505 nm, the quadratic relation indicates there are two $Yb^{3+}$ ions involved in this process. Although the transition of $^1G_4 \rightarrow {}^3H_6$ of $Tm^{3+}$ gives rise to blue-green emission around 488 nm, which is easily confused with the CL of the $Yb^{3+}$–$Yb^{3+}$ pair, the population of the upper $^1G_4$ level is a three-photon process.[4,35] Therefore, this emission band originates directly from the $Yb^{3+}$–$Yb^{3+}$ pair.

To further confirm our assignments, the fluorescence decay curves were also measured and analyzed, which is thought to be able to unambiguously investigate the underlying mechanisms. Figure 7 shows the normalized fluorescence decay curves of the Stokes 1040 and anti-Stokes 505 nm emissions for the sample

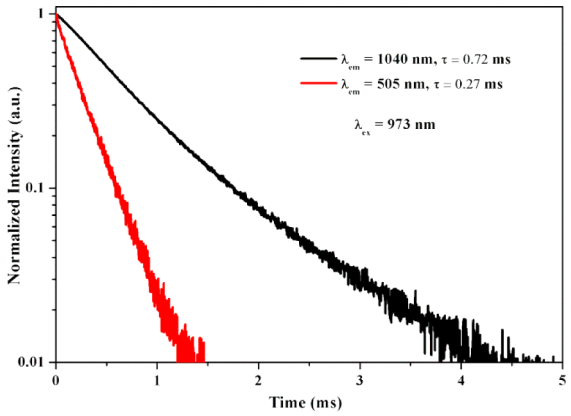


**Figure 7.** Fluorescence decay curves of $Yb^{3+}$ luminescence for CSS:0.3Yb,0.003Tb monitoring at 1040 and 505 nm, respectively, upon excitation by short-pulsed 973 nm laser.

CSS:0.3Yb,0.003Tb, excited by short-pulsed 973 nm laser. The decay curve of isolated $Yb^{3+}$ (1040 nm) is nearly exponential with the decay time of 0.72 ms. The decay time of anti-Stokes 505 nm emission is 0.27 ms, almost half of that of the Stokes 1040 nm emission, as expected from the rate equation model for the cooperative process.[24,24,37] More importantly, the decay curve of 505 nm emission shows no observable rise time, indicating the absence of an energy transfer process for this emission. Consequently, it is confirmed that the emission band around 505 nm originates from the CL of the $Yb^{3+}$–$Yb^{3+}$ pair.

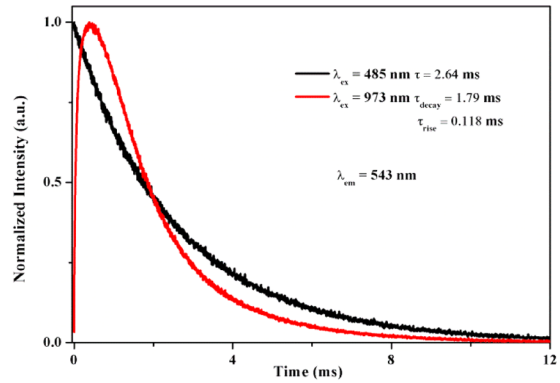


**Figure 8.** Fluorescence decay curves of $Tb^{3+}{}^5D_4$ luminescence (543 nm) for CSS:0.3Yb,0.24Tb upon excitation by 485 and 973 nm short-pulsed lasers, respectively.

Figure 8 shows the normalized fluorescence decay curves of $^5D_4$ luminescence (543 nm) of $Tb^{3+}$ for the CSS:0.3Yb,0.24Tb, excited by 485 and 973 nm short-pulsed lasers, respectively. As can be seen, upon the direct excitation of 485 nm, the decay curve presents a monotonously exponential decrease, while upon the UC excitation of 973 nm the decay curve shows an obvious rise time followed by a nearly exponential decrease. The rise time after laser pulse is a fingerprint of energy transfer process. Furthermore, for CET, the rise is related to the decay time of the $Yb^{3+}$–$Yb^{3+}$ pair, whereas the decay should be related to the decay time of $Tb^{3+}$. As proposed by Salley et al., the decay curve can be fitted by the following equation

$$I(t) = A[e^{-t/\tau_{decay}} - e^{-t/\tau_{rise}}]$$

where $\tau_{rise}$ and $\tau_{decay}$ represent the rise and decay times, respectively.[21] The rise time $\tau_{rise}$ was determined to be 0.118 ms, which is of the order of that of the CL at 505 nm, indicating that the first step population of $Tb^{3+}$ ($^5D_4$) is due to the CET from the $Yb^{3+}$–$Yb^{3+}$ pair. The obtained decay time of $Tb^{3+}$ in the UC process is 1.79 ms, which is slightly shorter than that of $Tb^{3+}$ upon direct excitation (2.64 ms). This difference is due to the preferential excitation in the UC process based on energy transfer. Specifically, in the UC excitation by 973 nm, those $Tb^{3+}$ ions having $Yb^{3+}$–$Yb^{3+}$ pairs as neighbors will be preferentially excited, whereas in the direct excitation of the $Tb^{3+}{}^5D_4$ level by 485 nm all the $Tb^{3+}$ ions are equally excited. Consequently, in UCL measurement, we detect only the luminescence from those $Tb^{3+}$ ions excited by the CET process, and in contrast, all the $Tb^{3+}$ ions are equally probed in downconversion luminescence measurement. Generally, since the energy transfer depends strongly on the distance between the participating ions, only a portion of ions with sufficiently


DOI: 10.1021/acs.jpcc.6b11633
J. Phys. Chem. C 2017, 121, 2998–3006

small interionic distances are able to participate in the energy transfer process. Hence, this phenomenon is common in UC systems based on energy transfer where the local environment of a subset of the activators differs greatly from that of the bulk due to the existence of a range of distances between neighboring ions.[18,20,33,65] In addition, the backward energy transfer from one $Tb^{3+}$ simultaneously to two $Yb^{3+}$ ions, known as quantum cutting, offers another decay avenue for the subset of $Tb^{3+}$ ions neighboring $Yb^{3+}$–$Yb^{3+}$ pairs, leading to a shorter decay time.[18−20,31,32] Finally, it should be noted that no detectable NIR emission around 1040 nm is observed when the $^5D_4$ level is directly excited by the light of 485 nm in the as-synthesized samples with various doping concentrations, although the green emission can be clearly detected. This means that the energy transfer processes from $Tb^{3+}$ to $Yb^{3+}$, such as CET and phonon-assisted energy transfer, are inefficient without preferential excitation.

## 4. CONCLUSION

In summary, we have obtained $RE^{3+}$ heavily doped single-phase silicate garnet CSS via the sol–gel method followed by high-temperature sintering. The results of Rietveld structural refinement indicate that multiple chemical unit substitutions of $[REO_8]$, $[AlO_6]$, and $[AlO_4]$, respectively, for $[CaO_8]$, $[ScO_6]$, and $[SiO_4]$ polyhedra can act as charge compensators for each other to promote the doping level of $RE^{3+}$ up to 20 mol %. Furthermore, in $Yb^{3+}$ and $Tb^{3+}$ heavily codoped CSS, intense cooperative UCL was observed and confirmed by the pump power dependence of the UCL intensity and the fluorescence decay curves. Structurally, antisite defects $Yb^{3+}$ for $Sc^{3+}$ and aliovalent substitution of $Yb^{3+}$ for $Ca^{2+}$ in CSS are both in favor of clustering into the closely spaced $Yb^{3+}$–$Yb^{3+}$ pair, markedly enhancing the efficiency of the cooperative UC process. Compared with the garnets YAG, YGG, and GGG, CSS has the highest UCL intensity when doping with 10 mol % $Yb^{3+}$ and 8 mol % $Tb^{3+}$, and its intensity is 37 times higher than that of YAG, making $Yb^{3+}$ and $Tb^{3+}$ codoped CSS a potential candidate for optical applications like tunable UC laser. Besides, the obtained single-phase CSS powder provides more possibilities for fabricating translucent or even transparent ceramic CSS; further research is under way in our group. More importantly, our results demonstrate that the multiple chemical unit cosubstitution is an effective strategy to promote the aliovalent substitution level or design solid solution materials to enhance or tune the luminescence properties where relatively high doping concentration is required.

## AUTHOR INFORMATION


### Corresponding Authors

*E-mail: zhangliangliang@ciomp.ac.cn.
*E-mail: zhangjh@ciomp.ac.cn.

### ORCID

Wenge Xiao: 0000-0002-3719-9434


### Notes

The authors declare no competing financial interest.

## ACKNOWLEDGMENTS

This work was partially supported by the National Key Research and Development Program of China (Grant No. 2016YFB0701003, 2016YFB0400605), National Natural Science Foundation of China (Grant No. 61275055, 11274007, 51402284, and 11604330), Natural Science Foundation of Jilin province (Grant No. 20140101169JC, 20150520022JH, and 20160520171JH), and the prior sci-tech program of innovation and entrepreneurship of oversea Chinese talent of Jilin province.

## REFERENCES


(1) Silversmith, A. J.; Lenth, W.; Macfarlane, R. M. Green Infrared-pumped Erbium Upconversion Laser. *Appl. Phys. Lett.* **1987**, *51*, 1977–1979.

(2) Moglia, F.; Müller, S.; Reichert, F.; Metz, P. W.; Calmano, T.; Kränkel, C.; Heumann, E.; Huber, G. Efficient Upconversion-pumped Continuous Wave $Er^{3+}$:$LiLuF_4$ Lasers. *Opt. Mater.* **2015**, *42*, 167–173.

(3) Zheng, W.; Huang, P.; Tu, D.; Ma, E.; Zhu, H.; Chen, X. Lanthanide-doped Upconversion Nano-bioprobes: Electronic Structures, Optical Properties, and Biodetection. *Chem. Soc. Rev.* **2015**, *44*, 1379–1415.

(4) Chen, G.; Ohulchanskyy, T. Y.; Kumar, R.; Ågren, H.; Prasad, P. N. Ultrasmall Monodisperse NaYF4:$Yb^{3+}$/$Tm^{3+}$ Nanocrystals with Enhanced Near-Infrared to Near-Infrared Upconversion Photoluminescence. *ACS Nano* **2010**, *4*, 3163–3168.

(5) Chen, D.; Yu, Y.; Huang, F.; Huang, P.; Yang, A.; Wang, Y. Modifying the Size and Shape of Monodisperse Bifunctional Alkaline-Earth Fluoride Nanocrystals through Lanthanide Doping. *J. Am. Chem. Soc.* **2010**, *132*, 9976–9978.

(6) Zhang, J.; Hao, Z.; Li, J.; Zhang, X.; Luo, Y.; Pan, G. Observation of Efficient Population of The Red-emitting State from the Green State by Non-multiphonon Relaxation in the $Er^{3+}$–$Yb^{3+}$ System. *Light: Sci. Appl.* **2015**, *4*, e239.

(7) Gao, W.; Wang, R.; Han, Q.; Dong, J.; Yan, L.; Zheng, H. Tuning Red Upconversion Emission in Single $LiYF_4$:$Yb^{3+}$/$Ho^{3+}$ Microparticle. *J. Phys. Chem. C* **2015**, *119*, 2349–2355.

(8) Feldmann, C.; Jüstel, T.; Ronda, C. R.; Schmidt, P. J. Inorganic Luminescent Materials: 100 Years of Research and Application. *Adv. Funct. Mater.* **2003**, *13*, 511–516.

(9) Zhou, X.; Zhang, Z.; Wang, Y. $Ce^{3+}$ and $Tb^{3+}$ Singly- and Co-doped $MgGd_4Si_3O_{13}$ for Ultraviolet Light Emitting Diodes and Field Emission Displays. *J. Mater. Chem. C* **2015**, *3*, 3676–3683.

(10) Lü, W.; Lv, W.; Zhao, Q.; Jiao, M.; Shao, B.; You, H. J. Generation of Orange and Green Emissions in $Ca_2GdZr_2(AlO_4)_3$:$Ce^{3+}$, $Mn^{2+}$, $Tb^{3+}$ Garnets via Energy Transfer with $Mn^{2+}$ and $Tb^{3+}$ as Acceptors. *J. Mater. Chem. C* **2015**, *3*, 2334–2340.

(11) Lin, C. C.; Chen, W.-T.; Chu, C.-I.; Huang, K.-W.; Yeh, C.-W.; Cheng, B.-M.; Liu, R.-S. UV/VUV Switch-driven Color-reversal Effect for Tb-activated Phosphors. *Light: Sci. Appl.* **2016**, *5*, e16066.

(12) Yamashita, T.; Ohishi, Y. Amplification and Lasing Characteristics of $Tb^{3+}$-doped Fluoride Fiber in the 0.54 μm Band. *Jpn. J. Appl. Phys.* **2007**, *46*, L991–L993.

(13) Yamashita, T.; Ohishi, Y. Optical Amplification at 0.54 μm by $Tb^{3+}$-doped Fluoride Fibre. *Electron. Lett.* **2007**, *43*, 88–90.

(14) Metz, P. W.; Marzahl, D.-T.; Majid, A.; Kränkel, C.; Hüber, G. Efficient Continuous Wave Laser Operation of $Tb^{3+}$-doped Fluoride Crystals in the Green and Yellow Spectral Regions. *Laser Photonics Rev.* **2016**, *10*, 335–344.

(15) Raue, R.; Nieuwesteeg, K.; Busselt, W. Saturation by Resonant Up-conversion in Tb-doped Phosphors. *J. Lumin.* **1991**, *48*, 485–488.

(16) dos Santos, J. F. M.; Terra, I. A. A.; Astrath, N. G. C.; Guimaraes, F. B.; Baesso, M. L.; Nunes, L. A. O.; Catunda, T. Mechanisms of Optical Losses in the $^5D_4$ and $^5D_3$ Levels in Tb3+ Doped Low Silica Calcium Aluminosilicate Glasses. *J. Appl. Phys.* **2015**, *117*, 53102.

(17) Noginov, M. A.; Venkateswarlu, P.; Mahdi, M. Two-step Upconversion Luminescence in Yb:Tb:YSGG Crystal. *J. Opt. Soc. Am. B* **1996**, *13*, 735–741.

(18) Yamashita, T.; Ohishi, Y. Analysis of Energy Transfers between $Tb^{3+}$ and $Yb^{3+}$ Codoped in Borosilicate Glasses. *J. Opt. Soc. Am. B* **2009**, *26*, 819–829.




DOI: 10.1021/acs.jpcc.6b11633
J. Phys. Chem. C 2017, 121, 2998–3006

(19) Arai, Y.; Yamashidta, T.; Suzuki, T.; Ohishi, Y. Upconversion Properties of $Tb^{3+}$–$Yb^{3+}$ Codoped Fluorophosphate Glasses. *J. Appl. Phys.* **2009**, *105*, 83105.
(20) Salley, G. M.; Valiente, R.; Güdel, H. U. Phonon-assisted cooperative sensitization of $Tb^{3+}$ in SrCl2:Yb,Tb. *J. Phys.: Condens. Matter* **2002**, *14*, 5461–5475.
(21) Salley, G. M.; Valiente, R.; Güdel, H. U. Luminescence Upconversion Mechanisms in $Yb^{3+}$–$Tb^{3+}$ Systems. *J. Lumin.* **2001**, *94*, 305–309.
(22) Nakazawa, E.; Shionoya, S. Cooperative Luminescence in YbPO4. *Phys. Rev. Lett.* **1970**, *25*, 1710–1712.
(23) Hehlen, M. P.; Güdel, H. U. Optical Spectroscopy of the Dimer System $Cs_3Yb_2Br_9$. *J. Chem. Phys.* **1993**, *98*, 1768–1775.
(24) Qin, W.-P.; Liu, Z.-Y.; Sin, C.-N.; Wu, C.-F.; Qin, G.-S.; Chen, Z.; Zheng, K.-Z. Multi-ion Cooperative Processes in $Yb^{3+}$ Clusters. *Light: Sci. Appl.* **2014**, *3*, e193.
(25) Wegh, R. T.; Meijerink, A. Cooperative Luminescence of Ytterbium(III) in $La_2O_3$. *Chem. Phys. Lett.* **1995**, *246*, 495–498.
(26) Goldner, P.; Schaudel, B.; Prassas, M. Dependence of Cooperative Luminescence Intensity on $Yb^{3+}$ Spatial Distribution in Crystals and Glasses. *Phys. Rev. B: Condens. Matter Mater. Phys.* **2002**, *65*, 54103.
(27) Ishii, T. First-principles Calculations for the Cooperative Transitions of $Yb^{3+}$ Dimer Clusters in $Y_3Al_5O_{12}$ and $Y_2O_3$ Crystals. *J. Chem. Phys.* **2005**, *122*, 24705.
(28) Dong, H.; Sun, L.-D.; Wang, Y.-F.; Xiao, J.-W.; Tu, D.; Chen, X.; Yan, C.-H. Photon Upconversion in $Yb^{3+}$–$Tb^{3+}$ and $Yb^{3+}$–$Eu^{3+}$ Activated Core/shell Nanoparticles with Dual-band Excitation. *J. Mater. Chem. C* **2016**, *4*, 4186–4192.
(29) Xue, M.; Zhu, X.; Qiu, X.; Gu, Y.; Feng, W.; Li, F. Highly Enhanced Cooperative Upconversion Luminescence through Energy Transfer Optimization and Quenching Protection. *ACS Appl. Mater. Interfaces* **2016**, *8*, 17894–17901.
(30) Xue, X.; Cheng, T.; Suzuki, T.; Ohishi, Y. Upconversion Emissions from High Energy Levels of $Tb^{3+}$ under Near-infrared Laser Excitation at 976 nm. *Opt. Mater. Express* **2015**, *5*, 2768–2776.
(31) Mishra, K.; Singh, S. K.; Singh, A. K.; Rai, M.; Gupta, B. K.; Rai, S. B. New Perspective in Garnet Phosphor: Low Temperature Synthesis, Nanostructures, and Observation of Multimodal Luminescence. *Inorg. Chem.* **2014**, *53*, 9561–9569.
(32) Grzyb, T.; Gruszeczka, A.; Wiglusz, R. J.; Lis, S. The Effects of Down- and Up-conversion on Dual-mode Green Luminescence from $Yb^{3+}$- and $Tb^{3+}$-doped $LaPO_4$ Nanocrystals. *J. Mater. Chem. C* **2013**, *1*, 5410–5418.
(33) Martín-Rodríguez, R.; Valiente, R.; Polizzi, S.; Bettinelli, M.; Speghini, A.; Piccinelli, F. Upconversion Luminescence in Nanocrystals of $Gd_3Ga_5O_{12}$ and $Y_3Al_5O_{12}$ Doped with $Tb^{3+}$-$Yb^{3+}$ and $Eu^{3+}$-$Yb^{3+}$. *J. Phys. Chem. C* **2009**, *113*, 12195–12200.
(34) Hehlen, M. P.; Kuditcher, A.; Rand, S. C.; Lüthi, S. R. Site-Selective, Intrinsically Bistable Luminescence of $Yb^{3+}$ Ion Pairs in $CsCdBr_3$. *Phys. Rev. Lett.* **1999**, *82*, 3050–3053.
(35) Noginov, M. A.; Loutts, G. B.; Steward, C. S.; Lucas, B. D.; Fider, D.; Peters, V.; Mix, E.; Hüber, G. Spectroscopic Study of Yb Doped Oxide Crystals for Intrinsic Optical Bistability. *J. Lumin.* **2002**, *96*, 129–140.
(36) Maciel, G. S.; Biswas, A.; Kapoor, R.; Prasad, P. N. Blue Cooperative Upconversion in Yb3+-doped Multicomponent Sol-gel-processed Silica Glass for Three-dimensional Display. *Appl. Phys. Lett.* **2000**, *76*, 1978–1980.
(37) Schaudel, B.; Goldner, P.; Prassas, M.; Auzel, F. Cooperative Luminescence as a Probe of Clustering in Yb Doped Glasses. *J. Alloys Compd.* **2000**, *300*, 443–449.
(38) Ikesue, A.; Aung, Y. L. Ceramic Laser Materials. *Nat. Photonics* **2008**, *2*, 721–727.
(39) Shi, Y.; Nikl, M.; Feng, X.; Mares, J. A.; Shen, Y.; Beitlerova, A.; Kucerkova, R.; Pan, Y.; Liu, Q. Microstructure, Optical, and Scintillation Characteristics of $Pr^{3+}$ Doped $Lu_3Al_5O_{12}$ Optical Ceramics. *J. Appl. Phys.* **2011**, *109*, 13522.
(40) Raukas, M.; Kelso, J.; Zheng, Y.; Bergenek, K.; Eisert, D.; Linkov, A.; Jermann, F. Ceramic Phosphors for Light Conversion in LEDs. *ECS J. Solid State Sci. Technol.* **2013**, *2*, R3168–R3176.
(41) Li, G.; Tian, Y.; Zhao, Y.; Lin, J. Recent Progress in Luminescence Tuning of $Ce^{3+}$ and $Eu^{2+}$-activated Phosphors for pc-WLEDs. *Chem. Soc. Rev.* **2015**, *44*, 8688–8713.
(42) Ji, H.; Wang, L.; Molokeev, M. S.; Hirosaki, N.; Huang, Z.; Xia, Z.; ten Kate, O. M.; Liu, L.; Xie, R. New Garnet Structure Phosphors, $Lu_{3x}Y_xMgAl_3SiO_{12}$:$Ce^{3+}$ ($x$ = 0–3), Developed by Solid Solution Design. *J. Mater. Chem. C* **2016**, *4*, 2359–2366.
(43) Thangadurai, V.; Narayanan, S.; Pinzaru, D. Garnet-type Solid-state Fast Li ion Conductors for Li Batteries: Critical Review. *Chem. Soc. Rev.* **2014**, *43*, 4714–4727.
(44) Shimomura, Y.; Honma, T.; Shigeiwa, M.; Akai, T.; Okamoto, K.; Kijima, N. Photoluminescence and Crystal Structure of Green-Emitting $Ca_3Sc_2Si_3O_{12}$:$Ce^{3+}$ Phosphor for White Light Emitting Diodes. *J. Electrochem. Soc.* **2007**, *154*, J35–J37.
(45) Suzuki, Y.; Kakihana, M.; Shimomura, Y.; Kijima, N. Synthesis of $Ca_3Sc_2Si_3O_{12}$:$Ce^{3+}$ Phosphor by Hydrothermal Si Alkoxide Gelation. *J. Mater. Sci.* **2008**, *43*, 2213–2216.
(46) Liu, Y.; Zhuang, W.; Hu, Y.; Gao, W.; Hao, J. Synthesis and Luminescence of Sub-micronSized $Ca_3Sc_2Si_3O_{12}$:Ce Green Phosphors for White Light-emitting Diode and Field-emission Display Applications. *J. Alloys Compd.* **2010**, *504*, 488–492.
(47) Wu, Y.-F.; Chan, Y.-H.; Nien, Y.-T.; Chen, I.-G. Crystal Structure and Optical Performance of $Al^{3+}$ and $Ce^{3+}$ Codoped $Ca_3Sc_2Si_3O_{12}$ Green Phosphors for White LEDs. *J. Am. Ceram. Soc.* **2013**, *96*, 234.
(48) Piccinelli, F.; Lausi, A.; Speghini, A.; Bettinelli, M. Crystal Structure Study of New Lanthanide Silicates with Silico-carnotite Structure. *J. Solid State Chem.* **2012**, *194*, 233–237.
(49) Rodrıguez-Carvajal, J. In *Satellite Meeting on Powder Diffraction of the 15th International Congress of the IUCr*, Toulouse (France), 1990.
(50) Geiger, C. A.; Armbruster, T. $Mn_3Al_2Si_3O_{12}$ Spessartine and $Ca_3Al_2Si_3O_{12}$ Grossular Garnet: Structural Dynamic and Thermodynamic Properties. *Am. Mineral.* **1997**, *82*, 740–747.
(51) Geller, S. Crystal Chemistry of the Garnets. *Z. Kristallogr. - Cryst. Mater.* **1967**, *125*, 1–47.
(52) Novak, G. A.; Gibbs, G. V. The Crystal Chemistry of the Silicate Garnets. *Am. Mineral.* **1971**, *56*, 791–825.
(53) Xia, Z.; Meijerink, A. $Ce^{3+}$-Doped Garnet Phosphors: Composition Modification, Luminescence Properties and Applications. *Chem. Soc. Rev.* **2017**, *46*, 275–299.
(54) Xia, Z.; Ma, C.; Molokeev, M. S.; Liu, Q.; Rickert, K.; Poeppelmeier, K. R. Chemical Unit Cosubstitution and Tuning of Photoluminescence in the $Ca_2(Al_{1-x}Mg_x)(Al_{1-x}Si_{1+x})O_7$:$Eu^{2+}$ Phosphor. *J. Am. Chem. Soc.* **2015**, *137*, 12494–12497.
(55) Wang, L.; Xie, R.-J.; Li, Y.; Wang, X.; Ma, C.-G.; Luo, D.; Takeda, T.; Tsai, Y.-T.; Liu, R.-S.; Hirosaki, N. $Ca_{1-x}Li_xAl_{1-x}Si_{1+x}N_3$:$Eu^{2+}$ Solid Solutions as Broadband, Color-tunable and Thermally Robust Red Phosphors for Superior Color Rendition White Light-emitting Diodes. *Light: Sci. Appl.* **2016**, *5*, e16155.
(56) Dai, P.-P.; Li, C.; Zhang, X.-T.; Xu, J.; Chen, X.; Wang, X.-L.; Jia, Y.; Wang, X.; Liu, Y.-C. A Single Eu2+-activated High-color-rendering Oxychloride White-light Phosphor for White-light-emitting Diodes. *Light: Sci. Appl.* **2016**, *5*, e16024.
(57) Shannon, R. D. Revised Effective Ionic Radii and Systematic Studies of Interatomic Distances in Halides and Chalcogenides. *Acta Crystallogr., Sect. A: Cryst. Phys., Diffr., Theor. Gen. Crystallogr.* **1976**, *32*, 751–767.
(58) Luo, Y.; Xia, Z. Effect of Al/Ga Substitution on Photoluminescence and Phosphorescence Properties of Garnet-Type $Y_3Sc_2Ga_{3-x}Al_xO_{12}$:$Ce^{3+}$ Phosphor. *J. Phys. Chem. C* **2014**, *118*, 23297–23305.
(59) Quartieri, S.; Chaboy, J.; Antonioli, G.; Geiger, C. A. XAFS Characterization of the Structural site of Yb in Synthetic Pyrope and Grossular garnets. II: XANES Full Multiple Scattering Calculations at the Yb LI-and LIII-edges. *Phys. Chem. Miner.* **1999**, *27*, 88–94.


DOI: 10.1021/acs.jpcc.6b11633
J. Phys. Chem. C 2017, 121, 2998–3006

(60) Akai, T.; Shigeiwa, M.; Okamoto, K.; Shimomura, Y.; Kijima, N.; Honma, T. In *X-RAY ABSORPTION FINE STRUCTURE-XAFS13:13th International Conference*; AIP Publishing, 2007; Vol. *882*, p 389.
(61) Zhou, R.; Wei, X.; Duan, C.; Chen, Y.; Yin, M. Intense Blue-green Cooperative Luminescence from Yb3+ Pairs within $CaNb_2O_6$ Matrix. *ECS J. Solid State Sci. Technol.* **2012**, *1*, R147−R152.
(62) Weber, M. J. Radiative and Multiphonon Relaxation of Rare-earth Ions in $Y_2O_3$. *Phys. Rev.* **1968**, *171*, 283−291.
(63) Ashurov, M. Kh.; Basiev, T. T.; Voron'ko, Yu. K.; Zharikov, E. V.; Zhekov, V. I.; Murina, T. M.; Osiko, V. V.; Timoshechkin, M. I.; Shcherbakov, I. A. Nonradiative Losses Due to the 4I11/2−4I13/2 Transition of the Er3+ Ion in $Y_3Al_5O_{12}$, $Gd_3Sc_2Al_3O_{12}$, $Y_3Ga_5O_{12}$, $Gd_3Ga_5O_{12}$, and $CaF_2$ Crystals. *Sov. J. Quantum Electron.* **1978**, *8*, 588−591.
(64) Pollnau, M.; Gamelin, D. R.; Luthi, S. R.; Güdel, H. U.; Hehlen, M. P. Power Dependence of Upconversion Luminescence in Lanthanide and Transition-metal-ion Systems. *Phys. Rev. B: Condens. Matter Mater. Phys.* **2000**, *61*, 3337−3346.
(65) Gamelin, D. R.; Güdel, H. U. Spectroscopy and Dynamics of $Re^{4+}$ Near-IR-to-visible Luminescence Upconversion. *Inorg. Chem.* **1999**, *38*, 5154−5164.



DOI: 10.1021/acs.jpcc.6b11633
*J. Phys. Chem. C* 2017, 121, 2998−3006